Spin-orbit torques in Co/Pt(111) and Mn/W(001) magnetic bilayers from first principles

Frank Freimuth,* Stefan Blügel, and Yuriy Mokrousov

Peter Grünberg Institut and Institute for Advanced Simulation, Forschungszentrum Jülich and JARA, 52425 Jülich, Germany

(Received 20 May 2013; revised manuscript received 28 October 2014; published 18 November 2014)

An applied electric current through a space-inversion asymmetric magnet induces spin-orbit torques (SOTs) on the magnetic moments, which holds much promise for future memory devices. We discuss general Green's function expressions suitable to compute the linear-response SOT in disordered ferromagnets. The SOT can be decomposed into an even and an odd component with respect to magnetization reversal, where in the limit of vanishing disorder the even SOT is given by the constant Berry curvature of the occupied states, while the odd part exhibits a divergence with respect to disorder strength. Within this formalism, we perform first-principles density-functional theory calculations of the SOT in Co/Pt(111) and Mn/W(001) magnetic bilayers. We find the even and odd torque components to be of comparable magnitude. Moreover, the odd torque depends strongly on an additional capping layer, while the even torque is less sensitive. We show that the even torque is nearly entirely mediated by spin currents in contrast to the odd torque, which can contain an important contribution not due to spin transfer. Our results are in agreement with experiments, showing that our linear-response theory is well-suited for the description of SOTs in complex ferromagnets.

DOI: 10.1103/PhysRevB.90.174423 PACS number(s): 72.25.Ba, 72.25.Mk, 71.70.Ej, 75.70.Tj

I. INTRODUCTION

The combination of spin-orbit interaction (SOI) and broken inversion symmetry gives rise to torques on the magnetization of ferromagnets if an electric current is applied [1,2]. These so-called spin-orbit torques (SOTs) arise from the exchange of angular momentum between the crystal lattice and the magnetization and enable control of the magnetic state of a single ferromagnetic layer, while conventional spin-transfer torque (STT) [3] devices exploit the exchange of spin angular momentum between two ferromagnetic layers with different magnetization directions.

SOTs can be observed experimentally both in periodic crystals—if the structure lacks inversion symmetry like in bulk (Ga,Mn)As with zinc-blende crystalline structure [4,5]—and in trilayers with structural inversion asymmetry, e.g., in AlO_x/Co/Pt [6–9] and MgO/CoFeB/Ta [10–12], where a ferromagnetic layer is asymmetrically sandwiched between a heavy-metal layer and an oxide layer and the applied current is parallel to the interfaces. The observation of magnetization switching by SOTs in systems with strong perpendicular anisotropy suggests promising new ways to realize magnetic memory devices [7,8].

Two qualitatively different SOTs are found in experiments on trilayers, one is an even function of magnetization direction $\hat{\mathbf{M}}$; the other one is an odd function. To lowest order in $\hat{\mathbf{M}}$, they are given by $\mathbf{T}^{\text{even}} = t^{\text{even}}\hat{\mathbf{M}} \times [(\hat{\mathbf{e}}_z \times \mathbf{E}) \times \hat{\mathbf{M}}]$ and $\mathbf{T}^{\text{odd}} = t^{\text{odd}}(\hat{\mathbf{e}}_z \times \mathbf{E}) \times \hat{\mathbf{M}}$, where $\mathbf{E}$ denotes the applied in-plane electric field and $\hat{\mathbf{e}}_z$ is a unit vector in the out-of-plane direction, i.e., perpendicular to the interfaces. Additional higher order terms describing the anisotropy of SOTs have been shown to be important in AlO_x/Co/Pt [13]. Inverse spin pumping [14] driven by the spin current due to the spin Hall effect (SHE) in the heavy-metal layer is expected to provide an important contribution to $\mathbf{T}^{\text{even}}$. Accordingly, it has been proposed to use materials with large spin Hall angles to achieve strong SOTs [10,15]. In trilayers, $\mathbf{T}^{\text{odd}}$ behaves like a fieldlike torque due to an effective magnetic field $\propto \hat{\mathbf{e}}_z \times \mathbf{E}$. Since $\hat{\mathbf{e}}_z \times \mathbf{E}$ is also the direction of the Rashba spin-orbit field for charge carriers moving along $\mathbf{E}$ in the structure inversion asymmetric geometry, one possible origin is the current-induced nonequilibrium spin accumulation along the spin-orbit field [16], which results—via the exchange interaction—in this effective magnetic field [1,17]. Indeed, the Rashba effect has been found to be strong at magnetic heavy-metal surfaces and interfaces [18,19]. Additionally, it is expected that part of $\mathbf{T}^{\text{odd}}$ arises from SHE and that part of $\mathbf{T}^{\text{even}}$ arises from the Rashba effect [20–22].

Understanding the roles played by the various mechanisms proposed to explain SOTs is crucial for optimizing and fine tuning their properties for future SOT-based devices. For this purpose we investigate in this work SOTs in Mn/W(001) and Co/Pt(111) bilayers as well as in O/Co/Pt(111) and Al/Co/Pt(111) trilayers using Kubo linear-response calculations based on the first-principles electronic structure obtained from density functional theory (DFT). Within a model description of disorder we study the dependence of SOTs on disorder strength. Additionally, we explore the dependence of the SOTs on the heavy-metal layer thickness. Furthermore, we determine to what extent spin currents mediate the torques by computing spin fluxes and decomposing the torque into contributions of individual atoms. By comparing SOTs in Mn/W(001) and Mn/W(001)/Mn we investigate the influence of an additional Mn substrate layer on the SOT. Finally, we compare the spin currents that contribute to the magnetic anisotropy torque to the spin currents that contribute to the SOT.

This article is structured as follows. We start with a discussion of the linear-response formalism used for the calculation of the SOT and specify the computational details in Sec. II. Section III presents the results. Atom-resolved torques and spin fluxes are introduced and investigated in Sec. III B. We conclude with a summary in Sec. IV. Additional derivations

*Corresponding author: f.freimuth@fz-juelich.de

and aspects related to the Kubo linear-response formalism for the SOT are given in the Appendixes.

II. COMPUTATIONAL METHOD

A. Kubo linear-response formalism for the torkance tensor

Within the local spin density approximation to DFT the Hamiltonian H can be decomposed as [23]

$$H = H_0 + \mu_B \boldsymbol{\sigma} \cdot \mathbf{\Omega}^{xc}, \tag{1}$$

where H_0 contains kinetic energy, scalar potential, and SOI. μ_B is the Bohr magneton, $\boldsymbol{\sigma} = (\sigma_x, \sigma_y, \sigma_z)^T$ is the vector of Pauli spin matrices, and $\mathbf{\Omega}^{xc}$ is the exchange field. We consider only ferromagnetic systems, where the exchange field $\mathbf{\Omega}^{xc}(\mathbf{r}) = \Omega^{xc}(\mathbf{r})\hat{\mathbf{M}}$ is characterized by a position-independent direction $\hat{\mathbf{M}}$ and a position-dependent amplitude $\Omega^{xc}(\mathbf{r})$. The relation to the Kohn-Sham effective potentials $V^{\text{eff}}_{\text{majority}}(\mathbf{r})$ and $V^{\text{eff}}_{\text{minority}}(\mathbf{r})$ of majority and minority electrons is given by $\Omega^{xc}(\mathbf{r}) = \frac{1}{2\mu_B}[V^{\text{eff}}_{\text{minority}}(\mathbf{r}) - V^{\text{eff}}_{\text{majority}}(\mathbf{r})]$. In response to an applied electric field a magnetization $\delta\mathbf{M}(\mathbf{r})$ is induced at position $\mathbf{r}$. As a consequence, the exchange field $\mathbf{\Omega}^{xc}(\mathbf{r})$ is modified by $\delta\mathbf{\Omega}^{xc}(\mathbf{r}) = \Omega^{xc}(\mathbf{r})\delta\mathbf{M}(\mathbf{r})/M(\mathbf{r})$. The resulting torque $\mathbf{T}$ on the magnetization within one unit cell is given by [24,25]

$$\mathbf{T} = \int d^3r \mathbf{M}(\mathbf{r}) \times \delta\mathbf{\Omega}^{xc}(\mathbf{r}) = \int d^3r \mathbf{\Omega}^{xc}(\mathbf{r}) \times \delta\mathbf{M}(\mathbf{r}), \tag{2}$$

where the integration is over the unit cell volume. Thus, the torque on the magnetization arises from the component of $\delta\mathbf{M}(\mathbf{r})$ that is perpendicular to $\mathbf{\Omega}^{xc}(\mathbf{r})$. Within linear-response theory the torque $\mathbf{T}$ arising due to an applied electric field $\mathbf{E}$ can be written as $\mathbf{T} = \mathbf{tE}$, which defines the torkance tensor $\mathbf{t}$. From the Kubo formalism we derive the expression $t_{ij} = t^{\text{I(a)}}_{ij} + t^{\text{I(b)}}_{ij} + t^{\text{II}}_{ij}$, where (see Appendix A)

$$\begin{aligned}
t^{\text{I(a)}}_{ij} &= \frac{e}{h} \text{Tr}\langle \mathcal{T}_i G^R(\mathcal{E}_F) v_j G^A(\mathcal{E}_F)\rangle, \\
t^{\text{I(b)}}_{ij} &= -\frac{e}{h} \text{Re Tr}\langle \mathcal{T}_i G^R(\mathcal{E}_F) v_j G^R(\mathcal{E}_F)\rangle, \\
t^{\text{II}}_{ij} &= \frac{e}{h} \int_{-\infty}^{\mathcal{E}_F} d\mathcal{E}\, \text{Re Tr}\left\langle \mathcal{T}_i G^R(\mathcal{E}) v_j \frac{dG^R(\mathcal{E})}{d\mathcal{E}} \right. \\
&\quad \left. - \mathcal{T}_i \frac{dG^R(\mathcal{E})}{d\mathcal{E}} v_j G^R(\mathcal{E}) \right\rangle.
\end{aligned} \tag{3}$$

Here $G^R(\mathcal{E})$ is the retarded Green's function, $G^A(\mathcal{E})$ is the advanced one, $\mathcal{E}_F$ is the Fermi energy, $e > 0$ is the elementary positive charge, and v_i is the ith Cartesian component of the velocity operator. The torque operator at position $\mathbf{r}$ is given by $\mathcal{T}(\mathbf{r}) = -\mu_B \boldsymbol{\sigma} \times \mathbf{\Omega}^{xc}(\mathbf{r})$, and $\mathcal{T}_i$ is its ith Cartesian component.

In order to compare theory with experiment, we decompose the computed torkance into its even and odd parts: $\mathbf{t}(\hat{\mathbf{M}}) = \mathbf{t}^{\text{even}}(\hat{\mathbf{M}}) + \mathbf{t}^{\text{odd}}(\hat{\mathbf{M}})$, where $\mathbf{t}^{\text{even}}(\hat{\mathbf{M}}) = [\mathbf{t}(\hat{\mathbf{M}}) + \mathbf{t}(-\hat{\mathbf{M}})]/2$ and $\mathbf{t}^{\text{odd}}(\hat{\mathbf{M}}) = [\mathbf{t}(\hat{\mathbf{M}}) - \mathbf{t}(-\hat{\mathbf{M}})]/2$. The same decomposition into even and odd parts is widely used in the case of the conductivity tensor $\sigma_{ij}(\hat{\mathbf{M}})$ [see also Eq. (A5)]: $\sigma_{ij}(\hat{\mathbf{M}}) = \sigma^{\text{even}}_{ij}(\hat{\mathbf{M}}) + \sigma^{\text{odd}}_{ij}(\hat{\mathbf{M}})$, where $\sigma^{\text{even}}_{ij}(\hat{\mathbf{M}}) = [\sigma_{ij}(\hat{\mathbf{M}}) + \sigma_{ij}(-\hat{\mathbf{M}})]/2$ and $\sigma^{\text{odd}}_{ij}(\hat{\mathbf{M}}) = [\sigma_{ij}(\hat{\mathbf{M}}) - \sigma_{ij}(-\hat{\mathbf{M}})]/2$. Due to the Onsager relation $\sigma_{ij}(\hat{\mathbf{M}}) = \sigma_{ji}(-\hat{\mathbf{M}})$ the even part of the conductivity tensor is symmetric, i.e., $\sigma^{\text{even}}_{ij}(\hat{\mathbf{M}}) = \sigma^{\text{even}}_{ji}(\hat{\mathbf{M}})$, while the odd part of the conductivity tensor is antisymmetric, i.e., $\sigma^{\text{odd}}_{ij}(\hat{\mathbf{M}}) = -\sigma^{\text{odd}}_{ji}(\hat{\mathbf{M}})$. [26] However, in the case of the SOTs, the Onsager reciprocity dictates that a time-dependent magnetization $\hat{\mathbf{M}}(t)$ induces a current density $\mathbf{j}(t) = [\mathbf{t}(-\hat{\mathbf{M}}(t))]^T[\hat{\mathbf{M}}(t) \times \frac{d\hat{\mathbf{M}}(t)}{dt}]/V$, where V is the unit cell volume [27]. Thus, while the Onsager reciprocity relates different matrix elements of the conductivity tensor, it does not relate different matrix elements of the torkance tensor, but instead relates the SOT to its inverse. Consequently, the even torkance is, in general, neither symmetric nor antisymmetric and likewise the odd torkance is, in general, neither symmetric nor antisymmetric.

We approximate the effect of disorder by a constant band broadening Γ, i.e., by setting $G^R(\mathcal{E}) = \hbar[\mathcal{E} - H + i\Gamma]^{-1}$, where H is the Hamiltonian Eq. (1) [28]. In the case of anomalous Hall effect (AHE) and SHE this constant Γ approximation does not capture the so-called side jump and skew scattering [29–33]. The computational assessment of formally analogous extrinsic contributions to the torkance is not considered here and left for future work. Within the constant Γ approximation the even torkance is given by (see Appendix A)

$$\begin{aligned}
t^{\text{even}}_{ij} = \frac{e\hbar}{2\pi\mathcal{N}} \sum_{\mathbf{k}n \neq m} &\text{Im}[\langle\psi_{\mathbf{k}n}|\mathcal{T}_i|\psi_{\mathbf{k}m}\rangle\langle\psi_{\mathbf{k}m}|v_j|\psi_{\mathbf{k}n}\rangle] \\
&\times \left\{ \frac{\Gamma(\mathcal{E}_{\mathbf{k}m} - \mathcal{E}_{\mathbf{k}n})}{[(\mathcal{E}_F - \mathcal{E}_{\mathbf{k}n})^2 + \Gamma^2][(\mathcal{E}_F - \mathcal{E}_{\mathbf{k}m})^2 + \Gamma^2]} \right. \\
&+ \frac{2\Gamma}{[\mathcal{E}_{\mathbf{k}n} - \mathcal{E}_{\mathbf{k}m}][(\mathcal{E}_F - \mathcal{E}_{\mathbf{k}m})^2 + \Gamma^2]} \\
&\left. + \frac{2}{[\mathcal{E}_{\mathbf{k}n} - \mathcal{E}_{\mathbf{k}m}]^2} \text{Im ln} \frac{\mathcal{E}_{\mathbf{k}m} - \mathcal{E}_F - i\Gamma}{\mathcal{E}_{\mathbf{k}n} - \mathcal{E}_F - i\Gamma} \right\}
\end{aligned} \tag{4}$$

and the odd torkance is given by

$$t^{\text{odd}}_{ij} = \frac{e\hbar}{\pi\mathcal{N}} \sum_{\mathbf{k}nm} \frac{\Gamma^2 \text{Re}[\langle\psi_{\mathbf{k}n}|\mathcal{T}_i|\psi_{\mathbf{k}m}\rangle\langle\psi_{\mathbf{k}m}|v_j|\psi_{\mathbf{k}n}\rangle]}{[(\mathcal{E}_F - \mathcal{E}_{\mathbf{k}n})^2 + \Gamma^2][(\mathcal{E}_F - \mathcal{E}_{\mathbf{k}m})^2 + \Gamma^2]}, \tag{5}$$

where $\mathcal{N}$ is the number of $\mathbf{k}$ points used to sample the Brillouin zone and $\psi_{\mathbf{k}n}$ and $\mathcal{E}_{\mathbf{k}n}$ denote the Bloch function for band n at $\mathbf{k}$ and the corresponding band energy, respectively.

It is instructive to consider the limit of $\Gamma \to 0$, where we obtain for the even torkance (see Appendix A)

$$t^{\text{even}}_{ij} \overset{\Gamma\to 0}{=} \frac{2e}{\mathcal{N}} \hat{\mathbf{e}}_i \cdot \sum_{\mathbf{k}} \sum_{n}^{\text{occ}} \left[\hat{\mathbf{M}} \times \text{Im} \left\langle \frac{\partial u_{\mathbf{k}n}}{\partial \hat{\mathbf{M}}} \middle| \frac{\partial u_{\mathbf{k}n}}{\partial k_j} \right\rangle \right] \tag{6}$$

and for the odd torkance

$$t^{\text{odd}}_{ij} \overset{\Gamma\to 0}{=} \frac{e\hbar}{2\Gamma\mathcal{N}} \sum_{\mathbf{k}n} \langle\psi_{\mathbf{k}n}|\mathcal{T}_i|\psi_{\mathbf{k}n}\rangle\langle\psi_{\mathbf{k}n}|v_j|\psi_{\mathbf{k}n}\rangle \delta(\mathcal{E}_F - \mathcal{E}_{\mathbf{k}n}). \tag{7}$$

In Eq. (6) $\hat{\mathbf{e}}_i$ denote the unit vectors in x, y, and z directions, where $\hat{\mathbf{e}}_x$ and $\hat{\mathbf{e}}_y$ are in the plane of the trilayers, the summation over band index n is restricted to the occupied (occ) states, and $u_{\mathbf{k}n}(\mathbf{r}) = e^{-i\mathbf{k}\cdot\mathbf{r}}\psi_{\mathbf{k}n}(\mathbf{r})$ is the lattice periodic part of the Bloch function $\psi_{\mathbf{k}n}(\mathbf{r})$. $\mathbf{t}^{\text{even}}$ is independent of Γ in the limit $\Gamma \to 0$ and describes the intrinsic contribution to the torkance. Like the intrinsic AHE [34] it has the form of a Berry curvature. This Berry curvature contribution to the SOT was recently observed in (Ga,Mn)As [5]. In contrast to $\mathbf{t}^{\text{even}}$, $\mathbf{t}^{\text{odd}}$ diverges like $\Gamma^{-1} = 2\tau/\hbar$ in the limit $\Gamma \to 0$, i.e., proportional to the relaxation time τ. A recent first-principles study [17] addressed the $\Gamma \to 0$ limit of $\mathbf{t}^{\text{odd}}$ in the case of Co/Pt bilayers.

Equations (4) and (5) are used in Sec. III to evaluate the SOT based on $\mathcal{T}_{\mathbf{k}inm} = \langle\psi_{\mathbf{k}n}|\mathcal{T}_i|\psi_{\mathbf{k}m}\rangle$, $v_{\mathbf{k}inm} = \langle\psi_{\mathbf{k}n}|v_i|\psi_{\mathbf{k}m}\rangle$, $\mathcal{E}_{\mathbf{k}m}$, and $\mathcal{E}_{\text{F}}$ obtained from first-principles electronic structure calculations. In order to converge the $\mathbf{k}$ summations in these expressions numerically efficiently, we made use of the Wannier interpolation technique [35]. Therefore, we first set up matrix elements of the necessary operators in the basis of maximally localized Wannier functions (MLWFs) [36]; i.e., we compute $\langle W_{n\mathbf{0}}|H|W_{m\mathbf{R}}\rangle$ and $\langle W_{n\mathbf{0}}|\mathcal{T}_i|W_{m\mathbf{R}}\rangle$, where $|W_{m\mathbf{R}}\rangle$ are the MLWFs. In order to obtain $\mathcal{T}_{\mathbf{k}inm}$, $v_{\mathbf{k}inm}$, and $\mathcal{E}_{\mathbf{k}m}$ at a given $\mathbf{k}$ point, we compute the Fourier transformations

$$\begin{aligned} H^{(\text{W})}_{\mathbf{k}nm} &= \sum_{\mathbf{R}} e^{i\mathbf{k}\cdot\mathbf{R}}\langle W_{n\mathbf{0}}|H|W_{m\mathbf{R}}\rangle, \\ v^{(\text{W})}_{\mathbf{k}inm} &= \frac{1}{\hbar}\sum_{\mathbf{R}} e^{i\mathbf{k}\cdot\mathbf{R}} i\text{R}_i\langle W_{n\mathbf{0}}|H|W_{m\mathbf{R}}\rangle, \\ \mathcal{T}^{(\text{W})}_{\mathbf{k}inm} &= \sum_{\mathbf{R}} e^{i\mathbf{k}\cdot\mathbf{R}}\langle W_{n\mathbf{0}}|\mathcal{T}_i|W_{m\mathbf{R}}\rangle, \end{aligned} \tag{8}$$

and transform them into the eigenstate representation according to

$$\begin{aligned} v_{\mathbf{k}inm} &= \sum_{n'm'} U^*_{\mathbf{k}n'n} v^{(\text{W})}_{\mathbf{k}in'm'} U_{\mathbf{k}m'm}, \\ \mathcal{T}_{\mathbf{k}inm} &= \sum_{n'm'} U^*_{\mathbf{k}n'n} \mathcal{T}^{(\text{W})}_{\mathbf{k}in'm'} U_{\mathbf{k}m'm}, \end{aligned} \tag{9}$$

where the columns of the matrix $U_{\mathbf{k}}$ are the eigenvectors of $H_{\mathbf{k}}$:

$$\sum_{m'} H_{\mathbf{k}nm'} U_{\mathbf{k}m'm} = \mathcal{E}_{\mathbf{k}m} U_{\mathbf{k}nm}. \tag{10}$$

B. Computational details

We performed DFT calculations of the electronic structure of Mn/W(001), where we considered a monolayer of Mn on 9 atomic layers of W [denoted in the following as Mn(1)/W(9)] and additionally a monolayer of Mn on 15 atomic layers of W [Mn(1)/W(15)]. In order to investigate the effect of a second ferromagnetic Mn layer on the torque, we also studied a Mn(1)/W(9)/Mn(1) trilayer, where 9 atomic layers of W(001) are symmetrically sandwiched between Mn monolayers on both sides. Structural parameters of the Mn/W(001) interface have been chosen, as determined in Ref. [37]. The asymmetric

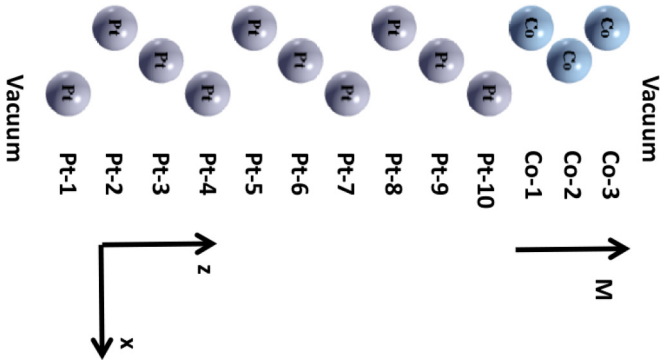

FIG. 1. (Color online) Illustration of the unit cell used in the thin film calculations of the Co/Pt(111) systems. Magnetization $\mathbf{M}$ is in z direction.

slabs were calculated with the film mode of the full-potential linearized augmented-plane-wave program FLEUR [38], which explicitly treats the vacuum region [39]. The plane wave cutoff was set to $4.1a_0^{-1}$, the muffin-tin (MT) radius of $2.42a_0$ (a_0 is Bohr's radius) was used for both Mn and W, and the generalized gradient approximation [40] was employed. We used a 24×24 Monkhorst-Pack [41] $\mathbf{k}$ mesh to sample the Brillouin zone in the self-consistent DFT calculations and treated SOI within second variation [42].

In the case of Co/Pt(111) bilayers we considered 3 layers of Co on 7 [Co(3)/Pt(7)], 10 [Co(3)/Pt(10)], 13 [Co(3)/Pt(13)], 15 [Co(3)/Pt(15)], and 20 [Co(3)/Pt(20)] atomic layers of Pt(111), corresponding to 1.6, 2.3, 3.0, 3.4, and 4.5 nm of Pt(111), respectively. We chose the (111) orientation for the fcc Pt layer since sputter deposited Pt typically shows a strong (111) texture along the growth direction [43]. In order to estimate roughly to what extent an oxide layer on the Co—like the AlO_x layer typically present in experiments—might influence the SOTs, we also considered thin films composed of 10 atomic layers of Pt(111), 3 atomic layers of Co, and 1 additional atomic layer of O or Al [denoted O(1)/Co(3)/Pt(10) and Al(1)/Co(3)/Pt(10), respectively]. The in-plane lattice constant of the hexagonal unit cell was set to the experimental value of bulk Pt(111) of $a/\sqrt{2} = 5.24a_0$, where $a = 7.41a_0$ is the lattice constant of the corresponding cubic fcc unit cell of bulk Pt. The corresponding distance between Pt atomic layers along the (111) direction is $a/\sqrt{3} = 4.283a_0$. For the Co layer we assumed hcp stacking and that the first two atomic layers of Co follow the fcc pattern of Pt(111) [44,45]; i.e., the stacking sequence in the Pt layer is ABC and the Co layer is stacked like ABAB onto the Pt layer with termination ABC. The unit cell used in the calculations is illustrated for the case of Co(3)/Pt(10) in Fig. 1. The O and Al atoms are deposited at the same in-plane position as Co-2. The plane wave cutoff was set to $3.7a_0^{-1}$ and the following MT radii were used: $2.5a_0$ for Pt, $1.8\,a_0$ for Co, $1.5a_0$ for Al, and $1.1a_0$ for O. Interfaces were relaxed in the out-of-plane direction. The resulting distance between the Pt-10 and Co-1 layers is $3.89a_0$, while the distance between adjacent Co layers is $3.50a_0$. The distances between the Co-3 and the optional Al and O capping layers are $3.82a_0$ and $1.84a_0$, respectively.

In order to evaluate Eqs. (4) and (5) computationally efficiently, we made use of the Wannier interpolation

technique. We constructed 18 MLWFs per transition metal atom, and additionally 8 MLWFs per O and Al atom using an 8×8 **k** mesh [46,47]. The subspace of the MLWFs was disentangled [48] from a number of bands of 1.4 times the number of desired MLWFs. A 1024×1024 Monkhorst-Pack [41] **k** mesh was used in the Wannier interpolation of Eqs. (4) and (5).

III. RESULTS

A. Total torkances

In Fig. 2 the torkances t_{yx}^{even} and t_{xx}^{odd} as obtained within the constant Γ model, Eqs. (4) and (5), respectively, are plotted for **M** in z direction. For this magnetization direction, the other components of the torkance tensor, t_{xx}^{even} and t_{yx}^{odd}, are zero due to the symmetries of the systems considered here (see Appendix B). As expected from Eq. (6), t_{yx}^{even} converges to its constant Berry curvature value in the limit $\Gamma \to 0$, while t_{xx}^{odd} scales like Γ^{-1} for small Γ, in agreement with Eq. (7). The sign of t_{yx}^{even} in all Co/Pt(111) systems studied here is positive, while the sign in the Mn/W(001) systems is negative. The positive sign of t_{yx}^{even} in the Co/Pt(111)-based systems is consistent with experiments [8,13]. The negative sign of t_{yx}^{even} in the Mn/W(001) systems agrees with experiments on a different W-based magnetic bilayer system, namely CoFeB/W [49]. The calculated even torkances t_{yx}^{even} in the Mn/W(001) systems agree in order of magnitude to those in the Co/Pt(111)-based systems. For broadening $\Gamma < 30$ meV the largest odd torkances t_{xx}^{odd} among the systems studied here are found for the Mn/W(001) systems, Al(1)/Co(3)/Pt(10) and O(1)/Co(3)/Pt(10).

Different heavy-metal layer thicknesses and cappings result in differences in the local electronic structure in the magnetic layer and at the interface between the heavy metal and the magnet. These differences are smeared out when the broadening Γ is large. Therefore, both t_{yx}^{even} and t_{xx}^{odd} become approximately independent of heavy-metal layer thickness and capping at large broadening Γ in both the Mn/W(001)-based and the Co/Pt(111)-based systems, while they vary substantially with layer thickness and capping at small Γ.

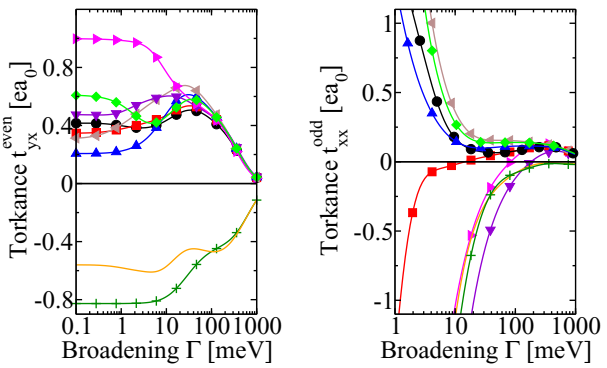

FIG. 2. (Color online) (a) Even torkance t_{yx}^{even} and (b) odd torkance t_{xx}^{odd} in Co(3)/Pt(7) (–●–), Co(3)/Pt(10) (–■–), Co(3)/Pt(13) (–◆–), Co(3)/Pt(15) (–▲–), Co(3)/Pt(20) (–◀–), Al(1)/Co(3)/Pt(10) (–▼–), O(1)/Co(3)/Pt(10) (–▶–), Mn(1)/W(9) (–+–), and Mn(1)/W(15) (——) for **M** in the z direction. The product of elementary positive charge e and Bohr radius a_0 used as unit of torkance amounts to $ea_0 = 8.478 \times 10^{-30}$ Cm.

The electrical resistivity of pure bulk Pt as measured experimentally at room temperature amounts to 10.6 $\mu\Omega$ cm. If we set $\Gamma = 25$ meV the resistivities [see also Eq. (A5)] obtained within the constant Γ model amount to $\rho_{xx} = 9.52$ $\mu\Omega$ cm [Co(3)/Pt(7)], $\rho_{xx} = 8.85$ $\mu\Omega$ cm [Co(3)/Pt(10)], $\rho_{xx} = 8.40$ $\mu\Omega$ cm [Co(3)/Pt(13)], $\rho_{xx} = 8.40$ $\mu\Omega$ cm [Co(3)/Pt(15)], $\rho_{xx} = 7.94$ $\mu\Omega$ cm [Co(3)/Pt(20)], $\rho_{xx} = 9.90$ $\mu\Omega$ cm [Al(1)/Co(3)/Pt(10)], and $\rho_{xx} = 10.65$ $\mu\Omega$ cm [O(1)/Co(3)/Pt(10)]. Thus, the constant Γ model reproduces roughly the electrical resistivity if we set the broadening to 25 meV. In order to estimate the torkance in the Co/Pt systems at room temperature within the constant Γ model, we therefore use $\Gamma = 25$ meV. Figure 1(a) shows that the deviation of t_{yx}^{even} from its $\Gamma \to 0$ limit is important at $\Gamma = 25$ meV for most of the systems studied here. In the Co/Pt(111) bilayer systems, t_{yx}^{even} increases with Pt thickness from $0.5ea_0$ in Co(3)/Pt(7) to $0.68ea_0$ in Co(3)/Pt(20) at $\Gamma = 25$ meV. Addition of an Al monolayer increases t_{yx}^{even} from $0.53ea_0$ in Co(3)/Pt(10) to $0.58ea_0$. Likewise, O(1)/Co(3)/Pt(10) has a higher t_{yx}^{even} of $0.62ea_0$ in comparison to Co(3)/Pt(10).

Experimentally, the SOT is often quantified in terms of the equivalent Oersted magnetic field that one would need to apply in order to produce the same torque on the magnetization like the SOT [6,7,9,11,12]. For a given torque **T** this magnetic field is $\mathbf{B} = (\mathbf{T} \times \hat{\mathbf{M}})/\mu_S$, where μ_S is the total spin magnetic moment in the unit cell. For this reason we discuss the torkance per spin magnetic moment, which amounts to $t_{yx}^{\text{even}}/\mu_S = 0.0141$ mT cm/V in O(1)/Co(3)/Pt(10) (10 atomic layers of Pt are 2.3 nm thick), in good agreement to the experimental result of 0.0139 mT cm/V in AlO_x(2 nm)/Co(0.6 nm)/Pt(3 nm) trilayers [50]. However, in Co(3)/Pt(13) (13 atomic layers of Pt are 3 nm thick) the torkance per spin magnetic moment $t_{yx}^{\text{even}}/\mu_S$ amounts to only 0.0091 mTcm/V. While $t_{yx}^{\text{even}} = 0.58ea_0$ in Co(3)/Pt(13) is smaller than t_{yx}^{even} in O(1)/Co(3)/Pt(10) by only 6%, the spin magnetic moment is reduced from $\mu_S = 5.78\mu_B$ in Co(3)/Pt(13) to $\mu_S = 4.02\mu_B$ in O(1)/Co(3)/Pt(10) due to the oxide layer. Thus, the increased $t_{yx}^{\text{even}}/\mu_S$ in O(1)/Co(3)/Pt(10) can be attributed mainly to the reduction of μ_S.

We now turn to the discussion of t_{xx}^{odd} in the Co/Pt(111) systems. The dependence on Pt thickness and capping at small values of the broadening Γ is overall stronger than in the case of t_{yx}^{even}. At $\Gamma = 25$ meV deposition of Al increases t_{xx}^{odd} in magnitude from $0.025ea_0$ in Co(3)/Pt(10) to $-0.835ea_0$, i.e., by roughly a factor of 30. Similarly, capping by an O layer increases t_{xx}^{odd} in magnitude to -0.372 ea_0. At larger values of Γ, t_{xx}^{odd} undergoes sign changes in Co(3)/Pt(10), O(1)/Co(3)/Pt(10), and Al(1)/Co(3)/Pt(10). The origin of both the strong variation with capping and the sign changes lies in the complexity of the interfacial spin-orbit coupling in realistic materials, where the sign of the effective Rashba parameter varies between different electronic bands leading to partial cancellation of contributions from bands with different effective Rashba parameters [17]. The torkance per

spin magnetic moment $t_{xx}^{\text{odd}}/\mu_S = -0.0085$ mT cm/V in O(1)/Co(3)/Pt(10) for $\Gamma = 25$ meV is in good agreement to the experimental value of -0.0089 mT cm/V [50] in nonannealed AlO_x(2 nm)/Co(0.6 nm)/Pt(3 nm) trilayers. In the uncapped Co/Pt(111) systems the magnitude of $t_{xx}^{\text{odd}}/\mu_S$ at $\Gamma = 25$ meV is smaller and the sign is opposite to experiment. According to our calculations, the oxidation of Co by the deposition of the AlO_x layer is thus crucial to obtain $t_{xx}^{\text{odd}}/\mu_S$ as measured experimentally in AlO_x(2 nm)/Co(0.6 nm)/Pt(3 nm).

W has been grown with resistivities as large as 80 and 260 $\mu\Omega$ cm in SOT experiments on CoFeB/W [49]. For the high-resistivity phase of W, large SHE angles have been reported. Therefore, we discuss the torkances in Mn/W(001) at a broadening of $\Gamma = 100$ meV. At this value of broadening we obtain within the constant Γ model resistivities of $\rho_{xx} = 69.4$ $\mu\Omega$ cm and of $\rho_{xx} = 60.2$ $\mu\Omega$ cm in Mn(1)/W(9) and Mn(1)/W(15), respectively. The corresponding torkances are $t_{yx}^{\text{even}} = -0.47ea_0$ and $t_{xx}^{\text{odd}} = -0.082ea_0$ in Mn(1)/W(9) and $t_{yx}^{\text{even}} = -0.47ea_0$ and $t_{xx}^{\text{odd}} = -0.085ea_0$ in Mn(1)/W(15). As torkances per spin magnetic moment we obtain $t_{yx}^{\text{even}}/\mu_S = -0.131$ mT cm/V and $t_{xx}^{\text{odd}}/\mu_S = -0.0229$ mT cm/V in Mn(1)/W(9) and $t_{yx}^{\text{even}}/\mu_S = -0.133$ mT cm/V and $t_{xx}^{\text{odd}}/\mu_S = -0.0241$ mT cm/V in Mn(1)/W(15). Sign and order of magnitude of t_{yx}^{even} agree to the experiment on CoFeB/W [49].

B. Atom-resolved torkances and spin-flux coefficients

In order to shed light on the mechanisms underlying the SOTs in magnetic bi- and trilayer films, we introduce the atom-resolved torkance $t_{ij\alpha}$, which we define by replacing $\mathcal{T}$ in Eq. (3) by the operator $\mathcal{T}_\alpha$, whose matrix elements are

$$\langle\psi_{\mathbf{k}n}|\mathcal{T}_\alpha|\psi_{\mathbf{k}m}\rangle = -\mu_B \int_{\text{MT}_\alpha} d^3r\, \psi_{\mathbf{k}n}^\dagger(\mathbf{r})\boldsymbol{\sigma} \times \boldsymbol{\Omega}^{\text{xc}}(\mathbf{r})\psi_{\mathbf{k}m}(\mathbf{r}), \tag{11}$$

where the volume integration is restricted to the MT sphere of the αth atom, which is denoted by MT_α. In contrast to $\mathcal{T}$, which measures the total torque acting on the magnetization within one unit cell, $\mathcal{T}_\alpha$ probes the torque on the spin magnetic moment of atom α. Since $\boldsymbol{\Omega}^{\text{xc}}(\mathbf{r})$ is much larger inside the MT spheres than between them, the sum of the atom-resolved torkances approximately yields the total torkance, i.e., $t_{ij} \approx \sum_\alpha t_{ij\alpha}$. Consequently, the torkance on the magnetization in the interstitial (INT) region between the MT spheres is small: $|t_{ij\text{INT}}| = |t_{ij} - \sum_\alpha t_{ij\alpha}| \ll |t_{ij}|$.

Additionally, we introduce the linear-response coefficients $q_{ij\alpha}$ of the flux of spin angular momentum [51] into the MT sphere of atom α. We define $q_{ij\alpha}$ by replacing $\mathcal{T}_i$ in Eq. (3) with the operator $\mathcal{Q}_{i\alpha}$, the matrix elements of which are given by

$$\langle\psi_{\mathbf{k}n}|\mathcal{Q}_{i\alpha}|\psi_{\mathbf{k}m}\rangle = -\frac{\mu_B\hbar}{2ie}\int_{S_\alpha} d\mathbf{S}\cdot[\psi_{\mathbf{k}n}^\dagger(\mathbf{r})\sigma_i\,\nabla\psi_{\mathbf{k}m}(\mathbf{r}) - \nabla\psi_{\mathbf{k}n}^\dagger(\mathbf{r})\sigma_i\,\psi_{\mathbf{k}m}(\mathbf{r})], \tag{12}$$

where the integration is performed over the surface S_α of the MT sphere of atom α. In the presence of SOI $q_{ij\alpha}$ generally differs from $t_{ij\alpha}$, because the spin current flux can be transferred both to the magnetization and to the lattice and because SOI generates additional torques that are not based on a spin current flux [1,2,52]. However, SOI is negligible in the interstitial region and the spin angular momentum flux into the interstitial region can therefore only be transferred to the interstitial magnetization and not to the lattice. Thus, we have to very good approximation $t_{ij\text{INT}} \approx q_{ij\text{INT}}$. This flux into the interstitial region is equal to the negative sum of the fluxes into the MT spheres, i.e., $q_{ij\text{INT}} = -\sum_\alpha q_{ij\alpha}$. Since we argued above that $|t_{ij\text{INT}}| \ll |t_{ij}|$, the sum of the fluxes $q_{ij\alpha}$ is likewise small, i.e., $|\sum_\alpha q_{ij\alpha}| \ll |t_{ij}|$. Additionally, due to translational invariance in the x and y directions, sizable contributions to $q_{ij\alpha}$ can only originate from spin currents flowing in the z direction. Thus, the spin fluxes $q_{ij\alpha}$ indicate by how much the nonequilibrium spin current flowing in the z direction is modified as it traverses the αth atomic layer.

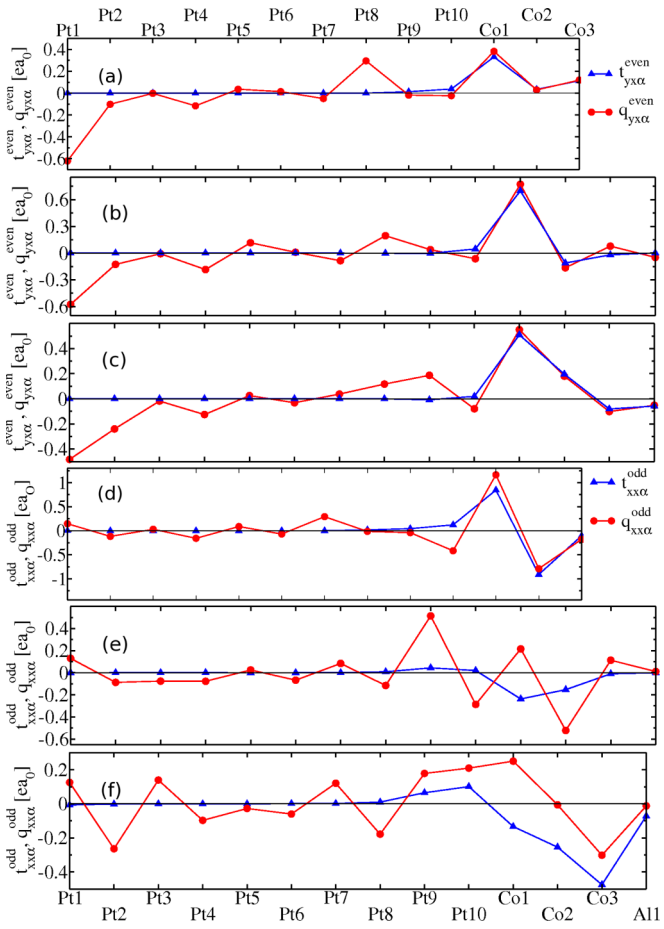

FIG. 3. (Color online) Atom-resolved torkance $t_{yx\alpha}^{\text{even}}$ (triangles) and atom-resolved spin-flux coefficient $q_{yx\alpha}^{\text{even}}$ (circles) in (a) Co(3)/Pt(10), (b) O(1)/Co(3)/Pt(10), and (c) Al(1)/Co(3)/Pt(10). Atom-resolved torkance $t_{xx\alpha}^{\text{odd}}$ (triangles) and atom-resolved spin-flux coefficient $q_{xx\alpha}^{\text{odd}}$ (circles) in (d) Co(3)/Pt(10), (e) O(1)/Co(3)/Pt(10), and (f) Al(1)/Co(3)/Pt(10). The broadening was set to $\Gamma = 25$ meV. Lines serve as guides for the eye.

In Figs. 3(a)–3(c) the atom-resolved torkances $t_{yx\alpha}^{\text{even}}$ and spin-flux coefficients $q_{yx\alpha}^{\text{even}}$ are shown for the systems Co(3)/Pt(10), O(1)/Co(3)/Pt(10), and Al(1)/Co(3)/Pt(10) at

$\Gamma = 25$ meV. $t^{\text{even}}_{yx\alpha}$ and $q^{\text{even}}_{yx\alpha}$ are obtained by replacing $\boldsymbol{\mathcal{T}}$ in Eq. (4) with $\boldsymbol{\mathcal{T}}_\alpha$ and $\boldsymbol{Q}_\alpha$, respectively. $t^{\text{even}}_{yx\alpha}$ (shown as triangles) is strongest at Co1 and negligibly small at Pt atoms. The difference between $t^{\text{even}}_{yx\alpha}$ and $q^{\text{even}}_{yx\alpha}$ (shown as circles) is insignificant at all three Co atoms. Thus, in the systems considered here, the even torkance $t^{\text{even}}_{yx\alpha}$ arises from the spin flux into the Co layer. In this regard, the even torque on the Co magnetization resembles the STT: In the case of STT in spin valves spin current is generated in one magnetic layer that acts as a polarizer and transferred to the magnetization of a second magnetic layer that acts as an analyzer [3]. In the Co/Pt(111) systems considered here, spin angular momentum flows from the nonmagnetic Pt layer into the Co layer, where it produces a torque on the magnetization.

The coefficient of spin flux into the Co layer, i.e., $q^{\text{even}}_{yx\text{Co1}} + q^{\text{even}}_{yx\text{Co2}} + q^{\text{even}}_{yx\text{Co3}}$, is positive. This implies a spin current with spin polarization along the $+y$ direction flowing in the $+z$ direction for an electric field along the $+x$ direction. This sign of the spin current agrees with the one of the intrinsic SHE of bulk Pt [8,53]. For α in the Pt layer $q^{\text{even}}_{yx\alpha}$ tends to be relatively small except for $\alpha = \text{Pt1}$. The coefficient $q^{\text{even}}_{yx\text{Pt1}}$ is negative and thus opposite in sign to the spin-flux coefficient on Co1. This negative spin flux into Pt1 arises from the absorption of spin current with spin polarization along the $-y$ direction flowing in the $-z$ direction, which is equivalent to spin current with spin polarization along the $+y$ direction flowing in the $+z$ direction. Hence, both the negative $q^{\text{even}}_{yx\text{Pt1}}$ and the positive $q^{\text{even}}_{yx\text{Co1}}$ are consistent with a spin current in Pt that is characterized by a spin polarization along $+y$ and flows in the $+z$ direction for electric field applied along the $+x$ direction. This spin current is absorbed efficiently by the magnetic Co1 atoms as well as by the nonmagnetic Pt1 atoms. The spin current absorbed at the Co1 atoms is transferred to the Co magnetization, while the spin current absorbed at the Pt1 atoms is transferred to the lattice via the SOI.

The situation is rather different for $t^{\text{odd}}_{xx\alpha}$ and $q^{\text{odd}}_{xx\alpha}$ shown in Figs. 3(d)–3(f). The cases of O(1)/Co(3)/Pt(10) and Al(1)/Co(3)/Pt(10) show clearly that, in general, the torkance on the Co moments differs significantly from the spin-flux coefficient. These differences between $t^{\text{odd}}_{xx\alpha}$ and $q^{\text{odd}}_{xx\alpha}$ for $\alpha = \text{Co1, Co2, Co3}$ result from the SOI on the Co atoms, which allows, on the one hand, the transfer of spin angular momentum flux to the lattice and, on the other hand, the generation of torques on the magnetization that are not related to a spin angular momentum flux. In the cases of Co(3)/Pt(10) and O(1)/Co(3)/Pt(10) the coefficients $q^{\text{odd}}_{xx\alpha}$ are very small for $\alpha = \text{Pt1}$ through $\alpha = \text{Pt8}$, in contrast to $q^{\text{even}}_{yx\alpha}$ discussed above, where, in particular, $q^{\text{even}}_{yx\text{Pt1}}$ is found to be sizable. This means that the spin fluxes that contribute to the odd torques in Co(3)/Pt(10) and O(1)/Co(3)/Pt(10) originate only close to the interface ($\alpha = \text{Pt9}$ and $\alpha = \text{Pt10}$). Thus, the interfacial spin-orbit coupling rather than the bulk Pt spin-orbit coupling contributes to the odd torque in Co(3)/Pt(10) and O(1)/Co(3)/Pt(10). In Al(1)/Co(3)/Pt(10) $q^{\text{odd}}_{xx\alpha}$ is sizable for $\alpha = \text{Pt1}$ through $\alpha = \text{Pt3}$, but $q^{\text{odd}}_{xx\alpha}$ oscillates in this region such that the sum of spin fluxes from the region $\alpha = \text{Pt1}$ through $\alpha = \text{Pt3}$ is negligible. Hence, the spin-flux contribution to the odd torque in Al(1)/Co(3)/Pt(10) originates also in this case from the Co/Pt interface region.

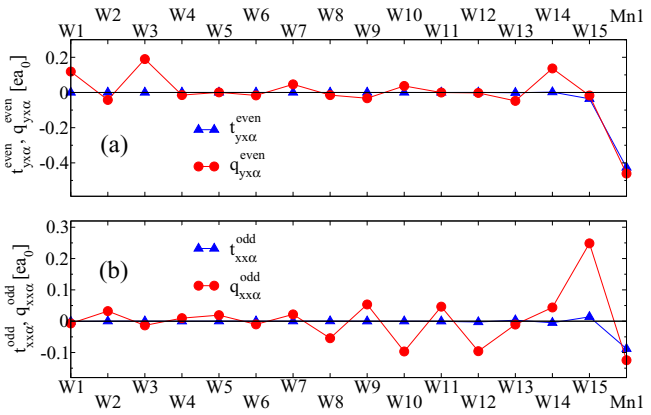

FIG. 4. (Color online) Atom-resolved torkances (triangles) and spin-flux coefficients (circles) in Mn(1)/W(15) at $\Gamma = 100$ meV. (a) $t^{\text{even}}_{yx\alpha}$ and $q^{\text{even}}_{yx\alpha}$; (b) $t^{\text{odd}}_{xx\alpha}$ and $q^{\text{odd}}_{xx\alpha}$.

Thus, the comparison of Figs. 3(a)–3(c) on the one hand to Figs. 3(d)–3(f) on the other hand corroborates the picture that the even torque in the Co/Pt system is associated with a spin current in Pt arising mainly from the bulk Pt SOI and flowing into the Co layer, while the odd torque is associated with interfacial spin-orbit coupling. While the electronic structure in the thin Pt layer differs from the one in bulk Pt, the bulk Pt SHE is predictive in both sign and order of magnitude for the spin current causing the even torque [8].

Figure 4 shows atom-resolved torkances and spin-flux coefficients in the Mn(1)/W(15) system. In the case of $t^{\text{even}}_{yx\alpha}$ and $q^{\text{even}}_{yx\alpha}$ shown in Fig. 4(a) we can identify a middle region ($\alpha = \text{W4}$ through $\alpha = \text{W13}$), where $q^{\text{even}}_{yx\alpha}$ is small. Large spin fluxes exist for the atoms W1 and W3 as well as for Mn1. The sign of the spin fluxes into W1 and W3 is opposite to the one for Mn1. Thus, the sign of these spin fluxes is consistent with a spin current with spin polarization along $-y$ flowing in the $+z$ direction if the electric field is applied along $+x$ direction. This spin current generates a torque on the magnetization of the Mn1 layer, whereby it is absorbed. Since the difference between $t^{\text{even}}_{yx\text{Mn1}}$ and $q^{\text{even}}_{yx\text{Mn1}}$ is small, the torque on Mn1 arises dominantly from the spin flux into the Mn1 sphere. The sign of the spin current generated in W is opposite to the one in Pt and consistent with the intrinsic SHE in bulk W [28,49]. On the other hand, $q^{\text{odd}}_{xx\alpha}$ shown in Fig. 4(b) is negligible in the region $\alpha = \text{W1}$ through $\alpha = \text{W7}$. The exchange of angular momentum between W and Mn that contributes to the odd torque is thus restricted to the interfacial region and can be attributed to the interfacial SOI. Since the difference between $t^{\text{odd}}_{xx\text{Mn1}}$ and $q^{\text{odd}}_{xx\text{Mn1}}$ is small, also the odd torque arises mostly from a spin flux in this case. In summary, the qualitative behavior of the atom-resolved torkances and spin-flux coefficients in the Mn(1)/W(15) system resembles the one in the Co(3)/Pt(10) system.

The large values of $q^{\text{even}}_{yx\text{Pt1}}$ and $q^{\text{even}}_{yx\text{W1}}$ in Figs. 3(a)–3(c) and Fig. 4(a), respectively, pose the question to which extent an additional substrate below the heavy-metal layer might influence the even torque, in particular if the heavy-metal layer is thin. In order to address this question, we computed atom-resolved torkances and spin-flux coefficients in Mn(1)/W(9)/Mn(1),

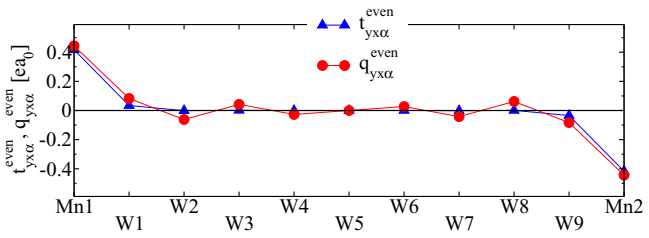

FIG. 5. (Color online) Atom-resolved torkance $t^{even}_{yx\alpha}$ (triangles) and atom-resolved spin-flux coefficient $q^{even}_{yx\alpha}$ (circles) in Mn(1)/W(9)/Mn(1) at $\Gamma = 100$ meV.

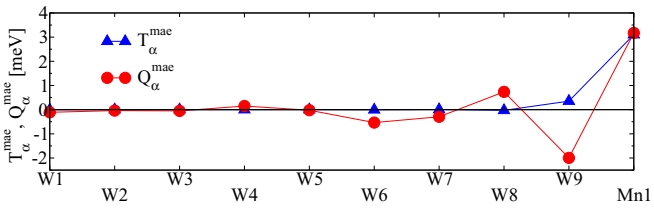

FIG. 6. (Color online) Atom-resolved torques (triangles) and spin-fluxes (circles) in Mn(1)/W(9) without applied electric field when the magnetization is rotated away from the easy axis by 30°.

which we show in Fig. 5. The magnetizations in the two Mn layers, Mn1 and Mn2, are chosen to be parallel to each other and along the z direction. Comparing Fig. 5 to Fig. 4(a) we find that in the Mn(1)/W(9)/Mn(1) system the additional magnetic layer (Mn1) absorbs the spin current with spin polarization along $+y$, which is flowing in the $-z$ direction, while in the Mn(1)/W(15) system it is absorbed by W1 and W3. Both absorption mechanisms are sufficiently efficient to prevent transformation of significant portions of the spin current flowing in the $-z$ direction into a spin current flowing in the $+z$ direction by reflection at the boundary of the system. Consequently, the resulting torkance $t^{even}_{yx\mathrm{Mn2}}$ in the Mn(1)/W(9)/Mn(1) system agrees well with the torkance $t^{even}_{yx\mathrm{Mn1}}$ in the Mn(1)/W(15) system.

The torkance t^{odd}_{ij} as given by Eq. (7) can be interpreted as a correction to the magnetic anisotropy due to the nonequilibrium distribution of electrons [2]. Without an applied electric field the torque due to magnetic anisotropy is given by [54]

$$\mathbf{T}^{\mathrm{mae}} = -\frac{1}{\mathcal{N}} \sum_{\mathbf{k}n} f_{\mathbf{k}n} \langle \psi_{\mathbf{k}n} | \boldsymbol{\mathcal{T}} | \psi_{\mathbf{k}n} \rangle, \tag{13}$$

where $f_{\mathbf{k}n}$ is 1 for occupied states and zero otherwise. Within the relaxation time approximation, an applied electric field $\mathbf{E}$ changes the occupancies $f_{\mathbf{k}n}$ by $\delta f_{\mathbf{k}n} = -e\tau \langle \psi_{\mathbf{k}n} | \mathbf{v} | \psi_{\mathbf{k}n} \rangle \cdot \mathbf{E}\, \delta(\mathcal{E}_{\mathrm{F}} - \mathcal{E}_{\mathbf{k}n})$, which modifies the torque by

$$-\frac{1}{\mathcal{N}} \sum_{\mathbf{k}n} \delta f_{\mathbf{k}n} \langle \psi_{\mathbf{k}n} | \mathcal{T}_i | \psi_{\mathbf{k}n} \rangle = \sum_j t^{\mathrm{odd}}_{ij} E_j, \tag{14}$$

where E_j are the Cartesian components of the applied electric field and t^{odd}_{ij} is given by Eq. (7). As discussed above, part of the odd torque is mediated by spin currents. In order to demonstrate that also the magnetic anisotropy torque, Eq. (13), can contain important contributions from spin currents in bilayer systems, we investigate the atom-resolved torques $\mathbf{T}^{\mathrm{mae}}_{\alpha}$ as well as the atom-resolved spin fluxes $\mathbf{Q}^{\mathrm{mae}}_{\alpha}$, which are obtained from Eq. (13) by replacing the torque operator $\boldsymbol{\mathcal{T}}$ by the atom-resolved torque operator $\boldsymbol{\mathcal{T}}_{\alpha}$, Eq. (11), and the atom-resolved spin flux $\boldsymbol{Q}_{\alpha}$, Eq. (12), respectively. Figure 6 shows $\mathbf{T}^{\mathrm{mae}}_{\alpha}$ and $\mathbf{Q}^{\mathrm{mae}}_{\alpha}$ in Mn(1)/W(9) when the magnetization is tilted away from the z axis towards the x axis by 30° (for magnetization along z, i.e., along the easy axis, both $\mathbf{T}^{\mathrm{mae}}_{\alpha}$ and $\mathbf{Q}^{\mathrm{mae}}_{\alpha}$ are zero). Clearly, the torque on Mn1 arises almost entirely from the spin flux. The spin fluxes $\mathbf{Q}^{\mathrm{mae}}_{\alpha}$ decay rapidly with increasing distance from the interface and are negligible on W1 through W5. This behavior resembles the one of the spin-flux coefficients $q^{odd}_{xx\alpha}$ shown in Fig. 4(b).

The electron wave functions are spinors $\psi_{\mathbf{k}n}(\mathbf{r}) = (\psi_{\mathbf{k}n\uparrow}(\mathbf{r}), \psi_{\mathbf{k}n\downarrow}(\mathbf{r}))^{\mathrm{T}}$, which do not carry any charge current in z direction. However, the spin-up and spin-down components of these spinors separately carry equal but opposite charge currents in the z direction. Thereby a spin current in the z direction is associated with each Bloch function $|\psi_{\mathbf{k}n}\rangle$. These spin currents in the z direction interact with the SOI as well as with the exchange field in Mn1 and close to the interface. Thereby, they exhibit the spin fluxes $\mathbf{Q}^{\mathrm{mae}}_{\alpha}$ shown in Fig. 6 and contribute to the magnetic anisotropy. This mechanism resembles the interlayer exchange coupling in spin valves or tunnel junctions, which is mediated by spin currents that flow between two magnets even in the absence of an applied bias [55,56]. In comparison to interlayer exchange coupling in spin valves, the SOI takes over the role of one of the two ferromagnets.

For magnetization along z individual states $|\psi_{\mathbf{k}n}\rangle$ in Eq. (13) exhibit nonzero torques $\langle \psi_{\mathbf{k}n} | \boldsymbol{\mathcal{T}} | \psi_{\mathbf{k}n} \rangle$ and spin fluxes $\langle \psi_{\mathbf{k}n} | \boldsymbol{Q}_{\alpha} | \psi_{\mathbf{k}n} \rangle$. However, the net torques and spin fluxes are zero when the Brillouin zone summation is carried out and when magnetization is along z. For this reason we tilted the magnetization direction away from the easy axis in Fig. 6. When an electric field is applied the states are occupied according to a nonequilibrium distribution and the Brillouin zone summation in Eq. (14) yields a nonzero torque even for magnetization along z. This explains the similar qualitative behavior of the odd spin-flux coefficients $q^{odd}_{xx\alpha}$ shown in Fig. 4(b) and the spin fluxes $\mathbf{Q}^{\mathrm{mae}}_{\alpha}$: The spin currents that contribute to the odd torque are present also without applied electric field. An additional electric field only changes the relative weight of the spin current associated with a given state $|\psi_{\mathbf{k}n}\rangle$ by changing its occupancy $f_{\mathbf{k}n}$. In contrast, the spin current due to SHE is not present without applied electric field, which is why the even spin-flux coefficients $q^{even}_{yx\alpha}$ differ qualitatively from $q^{odd}_{xx\alpha}$.

IV. SUMMARY

We performed first-principles calculations of the SOTs in Co/Pt(111) and Mn/W(001) within the Kubo linear-response formalism. We decomposed the SOTs into their even and odd contributions with respect to magnetization reversal, because these even and odd parts depend differently on disorder, which

we approximated by a constant band broadening. Moreover, in the bi- and trilayer systems considered here, the even torque arises dominantly from bulk spin-orbit coupling in the heavy-metal layer, while the odd torque depends strongly on the interfacial spin-orbit coupling. Moreover, we found that the even and the odd torques can be of similar magnitude, but that the odd torque can be suppressed due to its strong dependence on details like the capping and the heavy-metal layer thickness. While the even torque is almost entirely explained by spin currents originating in the heavy-metal layer and flowing into the magnetic layer, the odd torque can contain a sizable contribution that does not stem from spin transfer. The spin currents which add to the odd torque are also present if no electric field is applied, in which case they contribute to the magnetic anisotropy. Our results are in satisfactory agreement with experimental measurements.

ACKNOWLEDGMENTS

We gratefully acknowledge discussions with G. Bihlmayer, P. Gambardella, K. Garello, and I. M. Miron, computing time on the supercomputers JUQUEEN and JUROPA at Jülich Supercomputing Center and funding under HGF-YIG Program No. VH-NG-513.

APPENDIX A: LINEAR-RESPONSE FORMALISM FOR THE TORKANCE

We can write the torque on the magnetization within one unit cell due to an electron in state $\psi(\mathbf{r})$ as

$$\begin{aligned}\mathbf{T}[\psi] &= -\mu_{\mathrm{B}}\int d^3r\,\boldsymbol{\Omega}^{\mathrm{xc}}(\mathbf{r})\times\psi(\mathbf{r})^{\dagger}\boldsymbol{\sigma}\psi(\mathbf{r})\\ &= \mu_{\mathrm{B}}\int d^3r\,\psi(\mathbf{r})^{\dagger}\boldsymbol{\sigma}\psi(\mathbf{r})\times\boldsymbol{\Omega}^{\mathrm{xc}}(\mathbf{r})\\ &= -\int d^3r\,\psi(\mathbf{r})^{\dagger}\boldsymbol{\mathcal{T}}(\mathbf{r})\psi(\mathbf{r}),\end{aligned}\tag{A1}$$

where $\boldsymbol{\mathcal{T}}(\mathbf{r}) = -\mu_{\mathrm{B}}\boldsymbol{\sigma}\times\boldsymbol{\Omega}^{\mathrm{xc}}(\mathbf{r})$ is the torque operator. According to Kubo linear-response theory [57], the torkance tensor is given by

$$t_{ij} = -\lim_{\mathcal{E}\to 0}\left[\frac{1}{\mathcal{E}}\,\mathrm{Im}\,\Pi_{ij}(\mathcal{E})\right],\tag{A2}$$

where $\Pi_{ij}(\mathcal{E})$ is e times the Fourier transform of the retarded torque-velocity correlation function:

$$\Pi_{ij}(\mathcal{E}) = -ie\int_0^{\infty} dt\,e^{\frac{i}{\hbar}\mathcal{E}t}\langle[\mathcal{T}_i(t),v_j(0)]_-\rangle.\tag{A3}$$

Following the standard recipe [57] to obtain retarded functions conveniently by analytical continuation of Matsubara functions, it is straightforward to derive the expressions

$$\begin{aligned}t_{ij}^{\mathrm{I(a)}} &= -\frac{e}{h}\int_{-\infty}^{\infty} d\mathcal{E}\frac{df(\mathcal{E})}{d\mathcal{E}}\quad \mathrm{Tr}\langle\mathcal{T}_i G^{\mathrm{R}}(\mathcal{E})v_j G^{\mathrm{A}}(\mathcal{E})\rangle_{\mathrm{c}},\\ t_{ij}^{\mathrm{I(b)}} &= \frac{e}{h}\int_{-\infty}^{\infty} d\mathcal{E}\frac{df(\mathcal{E})}{d\mathcal{E}}\mathrm{ReTr}\langle\mathcal{T}_i G^{\mathrm{R}}(\mathcal{E})v_j G^{\mathrm{R}}(\mathcal{E})\rangle_{\mathrm{c}},\\ t_{ij}^{\mathrm{II}} &= \frac{e}{h}\int_{-\infty}^{\infty} d\mathcal{E}\,f(\mathcal{E})\quad \mathrm{ReTr}\langle\mathcal{T}_i G^{\mathrm{R}}(\mathcal{E})v_j\frac{dG^{\mathrm{R}}(\mathcal{E})}{d\mathcal{E}}\\ &\quad -\mathcal{T}_i\frac{dG^{\mathrm{R}}(\mathcal{E})}{d\mathcal{E}}v_j G^{\mathrm{R}}(\mathcal{E})\rangle_{\mathrm{c}},\end{aligned}\tag{A4}$$

which give the torkance as a sum of three terms, $t_{ij} = t_{ij}^{\mathrm{I(a)}} + t_{ij}^{\mathrm{I(b)}} + t_{ij}^{\mathrm{II}}$, the first two of which are Fermi surface terms, while the third one is a Fermi sea term. We assume that the dominant effect of room temperature on the torkance is the enhancement of the band broadening Γ. Therefore, we set the temperature of the Fermi-Dirac distribution function $f(\mathcal{E})$ to zero in the calculations. Replacing in Eq. (A4) $f(\mathcal{E})$ with the Heaviside step function $\theta(\mathcal{E}_{\mathrm{F}}-\mathcal{E})$ and $\frac{df(\mathcal{E})}{d\mathcal{E}}$ with the Dirac δ function $-\delta(\mathcal{E}_{\mathrm{F}}-\mathcal{E})$ leads to Eq. (3) in the main text.

The result Eq. (A4) can also be obtained from the Bastin equation [58,59] for the conductivity tensor,

$$\begin{aligned}\sigma_{ij}^{\mathrm{I(a)}} &= -\frac{e^2}{hV}\int_{-\infty}^{\infty} d\mathcal{E}\frac{df(\mathcal{E})}{d\mathcal{E}}\quad \mathrm{Tr}\langle v_i G^{\mathrm{R}}(\mathcal{E})v_j G^{\mathrm{A}}(\mathcal{E})\rangle_{\mathrm{c}},\\ \sigma_{ij}^{\mathrm{I(b)}} &= \frac{e^2}{hV}\int_{-\infty}^{\infty} d\mathcal{E}\frac{df(\mathcal{E})}{d\mathcal{E}}\mathrm{ReTr}\langle v_i G^{\mathrm{R}}(\mathcal{E})v_j G^{\mathrm{R}}(\mathcal{E})\rangle_{\mathrm{c}},\\ \sigma_{ij}^{\mathrm{II}} &= \frac{e^2}{hV}\int_{-\infty}^{\infty} d\mathcal{E}\,f(\mathcal{E})\quad \mathrm{ReTr}\langle v_i G^{\mathrm{R}}(\mathcal{E})v_j\frac{dG^{\mathrm{R}}(\mathcal{E})}{d\mathcal{E}}\\ &\quad - v_i\frac{dG^{\mathrm{R}}(\mathcal{E})}{d\mathcal{E}}v_j G^{\mathrm{R}}(\mathcal{E})\rangle_{\mathrm{c}},\end{aligned}\tag{A5}$$

by replacing the current density operator $-ev_i/V$ with $-\mathcal{T}_i$.

Within the constant Γ model it is convenient to use the eigenstate representation, i.e., $G^{\mathrm{R}}_{\mathbf{k}n}(\mathcal{E}) = \hbar[\mathcal{E}-\mathcal{E}_{\mathbf{k}n}+i\Gamma]^{-1}$. The eigenstate representation allows us to split Eq. (3) into two terms: one term, which contains only contributions of $\mathrm{Re}[\langle\psi_{\mathbf{k}n}|\mathcal{T}_i|\psi_{\mathbf{k}m}\rangle\langle\psi_{\mathbf{k}m}|v_j|\psi_{\mathbf{k}n}\rangle]$ and a second term containing only contributions of $\mathrm{Im}[\langle\psi_{\mathbf{k}n}|\mathcal{T}_i|\psi_{\mathbf{k}m}\rangle\langle\psi_{\mathbf{k}m}|v_j|\psi_{\mathbf{k}n}\rangle]$. The first term is given by

$$t_{ij}^{\mathrm{odd}} = \frac{e\hbar}{\pi\mathcal{N}}\sum_{\mathbf{k}nm}\frac{\Gamma^2\mathrm{Re}[\langle\psi_{\mathbf{k}n}|\mathcal{T}_i|\psi_{\mathbf{k}m}\rangle\langle\psi_{\mathbf{k}m}|v_j|\psi_{\mathbf{k}n}\rangle]}{[(\mathcal{E}_{\mathrm{F}}-\mathcal{E}_{\mathbf{k}n})^2+\Gamma^2][(\mathcal{E}_{\mathrm{F}}-\mathcal{E}_{\mathbf{k}m})^2+\Gamma^2]}.\tag{A6}$$

Only the Fermi surface terms in Eq. (A4), i.e., $t_{ij}^{\mathrm{I(a)}}$ and $t_{ij}^{\mathrm{I(b)}}$, contribute to t_{ij}^{odd}. Using the transformation properties under time reversal,

$$\begin{aligned}\boldsymbol{\Omega}^{\mathrm{xc}} &\to -\boldsymbol{\Omega}^{\mathrm{xc}},\\ \langle\psi_{\mathbf{k}n}|\mathbf{v}|\psi_{\mathbf{k}m}\rangle &\to -(\langle\psi_{\mathbf{k}n}|\mathbf{v}|\psi_{\mathbf{k}m}\rangle)^*,\\ \langle\psi_{\mathbf{k}n}|\mathbf{m}|\psi_{\mathbf{k}m}\rangle &\to -(\langle\psi_{\mathbf{k}n}|\mathbf{m}|\psi_{\mathbf{k}m}\rangle)^*,\\ \langle\psi_{\mathbf{k}n}|\boldsymbol{\mathcal{T}}|\psi_{\mathbf{k}m}\rangle &\to (\langle\psi_{\mathbf{k}n}|\boldsymbol{\mathcal{T}}|\psi_{\mathbf{k}m}\rangle)^*,\end{aligned}\tag{A7}$$

it is straightforward to show that the torkance component $t_{ij}^{\rm odd}$ is odd with respect to magnetization reversal. The second term yields

$$t_{ij}^{\rm even} = \frac{e\hbar}{2\pi\mathcal{N}} \sum_{\mathbf{k}n\neq m} \mathrm{Im}[\langle\psi_{\mathbf{k}n}|\mathcal{T}_i|\psi_{\mathbf{k}m}\rangle\langle\psi_{\mathbf{k}m}|v_j|\psi_{\mathbf{k}n}\rangle] \times \left\{ \frac{\Gamma(\mathcal{E}_{\mathbf{k}m}-\mathcal{E}_{\mathbf{k}n})}{[(\mathcal{E}_{\rm F}-\mathcal{E}_{\mathbf{k}n})^2+\Gamma^2][(\mathcal{E}_{\rm F}-\mathcal{E}_{\mathbf{k}m})^2+\Gamma^2]} + \frac{2\Gamma}{[\mathcal{E}_{\mathbf{k}n}-\mathcal{E}_{\mathbf{k}m}][(\mathcal{E}_{\rm F}-\mathcal{E}_{\mathbf{k}m})^2+\Gamma^2]} + \frac{2}{[\mathcal{E}_{\mathbf{k}n}-\mathcal{E}_{\mathbf{k}m}]^2}\mathrm{Im}\ln\frac{\mathcal{E}_{\mathbf{k}m}-\mathcal{E}_{\rm F}-i\Gamma}{\mathcal{E}_{\mathbf{k}n}-\mathcal{E}_{\rm F}-i\Gamma}\right\}. \quad \text{(A8)}$$

Only $t_{ij}^{\rm I(a)}$ and $t_{ij}^{\rm II}$ contribute to $t_{ij}^{\rm even}$. From Eq. (A7) it follows that $t_{ij}^{\rm even}$ is even with respect to magnetization reversal.

The odd torkance becomes in the limit $\Gamma \to 0$

$$t_{ij}^{\rm odd} \overset{\Gamma\to 0}{=} \frac{e\hbar}{2\Gamma\mathcal{N}} \sum_{\mathbf{k}n} \langle\psi_{\mathbf{k}n}|\mathcal{T}_i|\psi_{\mathbf{k}n}\rangle\langle\psi_{\mathbf{k}n}|v_j|\psi_{\mathbf{k}n}\rangle\delta(\mathcal{E}_{\rm F}-\mathcal{E}_{\mathbf{k}n}), \quad \text{(A9)}$$

which diverges like $1/\Gamma$. On the other hand, we obtain in the limit $\Gamma \to 0$

$$t_{ij}^{\rm even} \overset{\Gamma\to 0}{=} \frac{2e\hbar}{\mathcal{N}} \sum_{\mathbf{k}} \sum_{n}^{\rm occ} \sum_{m\neq n} \mathrm{Im}\left[\frac{\langle\psi_{\mathbf{k}n}|\mathcal{T}_i|\psi_{\mathbf{k}m}\rangle\langle\psi_{\mathbf{k}m}|v_j|\psi_{\mathbf{k}n}\rangle}{(\mathcal{E}_{\mathbf{k}m}-\mathcal{E}_{\mathbf{k}n})^2}\right], \quad \text{(A10)}$$

where the summation over band index n is restricted to the occupied (occ) bands. This expression is independent of Γ and thus describes the intrinsic contribution to the torkance.

According to Eq. (1) the Hamiltonian H is dependent on the magnetization direction $\hat{\mathbf{M}}$ through the exchange interaction $\mu_{\rm B}\boldsymbol{\sigma}\cdot\hat{\mathbf{M}}\,\Omega^{\rm xc}(\mathbf{r})$. The derivative of H with respect to magnetization direction $\hat{\mathbf{M}}$ is related to the torque operator as follows:

$$\hat{\mathbf{M}}\times\frac{\partial H}{\partial\hat{\mathbf{M}}} = \mu_{\rm B}\hat{\mathbf{M}}\times\boldsymbol{\sigma}\,\Omega^{\rm xc}(\mathbf{r}) = -\mu_{\rm B}\boldsymbol{\sigma}\times\boldsymbol{\Omega}^{\rm xc}(\mathbf{r}) = \boldsymbol{\mathcal{T}}(\mathbf{r}). \quad \text{(A11)}$$

Using

$$\frac{\partial|u_{\mathbf{k}n}\rangle}{\partial k_j} = \sum_{m\neq n}\frac{|u_{\mathbf{k}m}\rangle\langle u_{\mathbf{k}m}|\frac{\partial H(\mathbf{k})}{\partial k_j}|u_{\mathbf{k}n}\rangle}{\mathcal{E}_{\mathbf{k}n}-\mathcal{E}_{\mathbf{k}m}} + ia_{\mathbf{k}nj}|u_{\mathbf{k}n}\rangle = \hbar\sum_{m\neq n}\frac{|u_{\mathbf{k}m}\rangle\langle u_{\mathbf{k}m}|v_j(\mathbf{k})|u_{\mathbf{k}n}\rangle}{\mathcal{E}_{\mathbf{k}n}-\mathcal{E}_{\mathbf{k}m}} + ia_{\mathbf{k}nj}|u_{\mathbf{k}n}\rangle \quad \text{(A12)}$$

and

$$\hat{\mathbf{M}}\times\frac{\partial|u_{\mathbf{k}n}\rangle}{\partial\hat{\mathbf{M}}} = \sum_{m\neq n}\frac{|u_{\mathbf{k}m}\rangle\langle u_{\mathbf{k}m}|\hat{\mathbf{M}}\times\frac{\partial H(\mathbf{k})}{\partial\hat{\mathbf{M}}}|u_{\mathbf{k}n}\rangle}{\mathcal{E}_{\mathbf{k}n}-\mathcal{E}_{\mathbf{k}m}} + ia_{\mathbf{k}n\mathcal{T}}|u_{\mathbf{k}n}\rangle = \sum_{m\neq n}\frac{|u_{\mathbf{k}m}\rangle\langle u_{\mathbf{k}m}|\boldsymbol{\mathcal{T}}|u_{\mathbf{k}n}\rangle}{\mathcal{E}_{\mathbf{k}n}-\mathcal{E}_{\mathbf{k}m}} + ia_{\mathbf{k}n\mathcal{T}}|u_{\mathbf{k}n}\rangle, \quad \text{(A13)}$$

where the phases $a_{\mathbf{k}nj}$ and $\mathbf{a}_{\mathbf{k}n\mathcal{T}}$ determine the gauge, $H(\mathbf{k}) = e^{-i\mathbf{k}\cdot\mathbf{r}}He^{i\mathbf{k}\cdot\mathbf{r}}$ is the Hamiltonian in crystal momentum representation and $u_{\mathbf{k}n}(\mathbf{r}) = e^{-i\mathbf{k}\cdot\mathbf{r}}\psi_{\mathbf{k}n}(\mathbf{r})$ is the lattice periodic part of the Bloch function $\psi_{\mathbf{k}n}(\mathbf{r})$, we obtain

$$t_{ij}^{\rm even} \overset{\Gamma\to 0}{=} \frac{2e}{\mathcal{N}}\hat{\mathbf{e}}_i\cdot\sum_{\mathbf{k}}\sum_{n}\left[\hat{\mathbf{M}}\times\mathrm{Im}\left\langle\frac{\partial u_{\mathbf{k}n}}{\partial\hat{\mathbf{M}}}\middle|\frac{\partial u_{\mathbf{k}n}}{\partial k_j}\right\rangle\right], \quad \text{(A14)}$$

which has the form of a Berry curvature similar to the AHE. However, this Berry curvature contribution to the SOT requires us to differentiate also with respect to the magnetization direction $\hat{\mathbf{M}}$ and not only with respect to $\mathbf{k}$. It is thus a mixed Berry curvature in $\mathbf{k}$-$\hat{\mathbf{M}}$ space. This mixed $\mathbf{k}$-$\hat{\mathbf{M}}$ Berry curvature has recently been shown to govern also the Dzyaloshinkii-Moriya interaction [60,61].

APPENDIX B: SYMMETRY CONSIDERATIONS

General symmetry properties of SOTs are discussed in Refs. [13,62,63]. In the films that we consider in this work, the xz plane is a mirror plane. For $\mathbf{M}$ in the z direction, mirror reflection at the xz plane inverts $\mathbf{M}$, because it is an axial vector. Likewise, the x component of the torque is inverted, but the y component is not, because also the torque is an axial vector. An electric field along the x direction is not inverted by mirror reflection at the xz plane, because the electric field is a polar vector. Consequently, symmetry requires t_{xx} to be an odd function of magnetization and t_{yx} to be an even function of magnetization for $\mathbf{M}$ in the z direction. Thus, $t_{xx}^{\rm even}=0$ and $t_{yx}^{\rm odd}=0$ if $\mathbf{M}$ is in the z direction. When the magnetization is in z direction the Mn/W(001) films considered in this work exhibit $c4$ symmetry around the z axis and the Co/Pt(111)-based films $c3$ symmetry. As a consequence of these rotational symmetries we have additionally $t_{yy}=t_{xx}=t_{xx}^{\rm odd}$ and $t_{xy}=-t_{yx}=-t_{yx}^{\rm even}$. Thus, for magnetization along the z direction we find the odd torkance to be a symmetric tensor and the even torkance to be an antisymmetric tensor. However, in general, the even torkance tensor is not always antisymmetric and the odd torkance tensor is not always symmetric. Symmetry and antisymmetry of the odd and even parts of the torkance tensor arise from the rotational symmetries of the systems that we consider here and not from the Onsager reciprocity relations of the torkance tensor.

[1] A. Manchon and S. Zhang, Phys. Rev. B **79**, 094422 (2009).
[2] I. Garate and A. H. MacDonald, Phys. Rev. B **80**, 134403 (2009).
[3] M. D. Stiles and J. Miltat, in *Spin Dynamics in Confined Magnetic Structures III*, Topics in Applied Physics Vol. 101 (Springer-Verlag, Berlin, 2006), p. 225.
[4] A. Chernyshov, M. Overby, X. Liu, J. K. Furdyna, Y. Lyanda-Geller, and L. P. Rokhinson, Nat. Phys. **5**, 656 (2009).
[5] H. Kurebayashi, J. Sinova, D. Fang, A. C. Irvine, T. D. Skinner, J. Wunderlich, V. Novák, R. P. Campion, B. L. Gallagher, E. K. Vehstedt *et al.*, Nat. Nanotechnol. **9**, 211 (2014).

[6] I. M. Miron, G. Gaudin, S. Auffret, B. Rodmacq, A. Schuhl, S. Pizzini, J. Vogel, and P. Gambardella, Nat. Mater. **9**, 230 (2010).

[7] I. Mihai Miron, K. Garello, G. Gaudin, P.-J. Zermatten, M. V. Costache, S. Auffret, S. Bandiera, B. Rodmacq, A. Schuhl, and P. Gambardella, Nature (London) **476**, 189 (2011).

[8] L. Liu, O. J. Lee, T. J. Gudmundsen, D. C. Ralph, and R. A. Buhrman, Phys. Rev. Lett. **109**, 096602 (2012).

[9] U. H. Pi, K. W. Kim, J. Y. Bae, S. C. Lee, Y. J. Cho, K. S. Kim, and S. Seo, Appl. Phys. Lett. **97**, 162507 (2010).

[10] L. Liu, C.-F. Pai, Y. Li, H. W. Tseng, D. C. Ralph, and R. A. Buhrman, Science **336**, 555 (2012).

[11] J. Kim, J. Sinha, M. Hayashi, M. Yamanouchi, S. Fukami, T. Suzuki, S. Mitani, and H. Ohno, Nat. Mater. **12**, 240 (2013).

[12] T. Suzuki, S. Fukami, N. Ishiwata, M. Yamanouchi, S. Ikeda, N. Kasai, and H. Ohno, Appl. Phys. Lett. **98**, 142505 (2011).

[13] K. Garello, I. M. Miron, C. O. Avci, F. Freimuth, Y. Mokrousov, S. Blügel, S. Auffret, O. Boulle, G. Gaudin, and P. Gambardella, Nat. Nanotechnol. **8**, 587 (2013).

[14] Y. Tserkovnyak, A. Brataas, and G. E. W. Bauer, Phys. Rev. B **66**, 224403 (2002).

[15] M. Gradhand, D. V. Fedorov, P. Zahn, I. Mertig, Y. Otani, Y. Niimi, L. Vila, and A. Fert, SPIN **02**, 1250010 (2012).

[16] V. Edelstein, Solid State Commun. **73**, 233 (1990).

[17] P. M. Haney, H.-W. Lee, K.-J. Lee, A. Manchon, and M. D. Stiles, Phys. Rev. B **88**, 214417 (2013).

[18] O. Krupin, G. Bihlmayer, K. Starke, S. Gorovikov, J. E. Prieto, K. Döbrich, S. Blügel, and G. Kaindl, Phys. Rev. B **71**, 201403 (2005).

[19] J.-H. Park, C. H. Kim, H.-W. Lee, and J. H. Han, Phys. Rev. B **87**, 041301 (2013).

[20] D. A. Pesin and A. H. MacDonald, Phys. Rev. B **86**, 014416 (2012).

[21] X. Wang and A. Manchon, Phys. Rev. Lett. **108**, 117201 (2012).

[22] P. M. Haney, H.-W. Lee, K.-J. Lee, A. Manchon, and M. D. Stiles, Phys. Rev. B **87**, 174411 (2013).

[23] P. Kurz, F. Förster, L. Nordström, G. Bihlmayer, and S. Blügel, Phys. Rev. B **69**, 024415 (2004).

[24] P. M. Haney, D. Waldron, R. A. Duine, A. S. Nunez, H. Guo, and A. H. MacDonald, Phys. Rev. B **76**, 024404 (2007).

[25] P. M. Haney, R. A. Duine, A. S. Nunez, and A. H. MacDonald, J. Magn. Magn. Mater. **320**, 1300 (2008).

[26] R. R. Birss, *Symmetry and Magnetism* (North-Holland, Amsterdam, 1964).

[27] F. Freimuth, S. Blügel, and Y. Mokrousov, arXiv:1406.3866.

[28] T. Tanaka, H. Kontani, M. Naito, T. Naito, D. S. Hirashima, K. Yamada, and J. Inoue, Phys. Rev. B **77**, 165117 (2008).

[29] S. Lowitzer, D. Ködderitzsch, and H. Ebert, Phys. Rev. Lett. **105**, 266604 (2010).

[30] I. Turek, J. Kudrnovský, and V. Drchal, Phys. Rev. B **86**, 014405 (2012).

[31] M. Gradhand, D. V. Fedorov, P. Zahn, and I. Mertig, Phys. Rev. Lett. **104**, 186403 (2010).

[32] A. A. Kovalev, J. Sinova, and Y. Tserkovnyak, Phys. Rev. Lett. **105**, 036601 (2010).

[33] J. Weischenberg, F. Freimuth, J. Sinova, S. Blügel, and Y. Mokrousov, Phys. Rev. Lett. **107**, 106601 (2011).

[34] N. Nagaosa, J. Sinova, S. Onoda, A. H. MacDonald, and N. P. Ong, Rev. Mod. Phys. **82**, 1539 (2010).

[35] J. R. Yates, X. Wang, D. Vanderbilt, and I. Souza, Phys. Rev. B **75**, 195121 (2007).

[36] N. Marzari, A. A. Mostofi, J. R. Yates, I. Souza, and D. Vanderbilt, Rev. Mod. Phys. **84**, 1419 (2012).

[37] P. Ferriani, S. Heinze, G. Bihlmayer, and S. Blügel, Phys. Rev. B **72**, 024452 (2005).

[38] See http://www.flapw.de

[39] H. Krakauer, M. Posternak, and A. J. Freeman, Phys. Rev. B **19**, 1706 (1979).

[40] J. P. Perdew, K. Burke, and M. Ernzerhof, Phys. Rev. Lett. **77**, 3865 (1996).

[41] H. J. Monkhorst and J. D. Pack, Phys. Rev. B **13**, 5188 (1976).

[42] C. Li, A. J. Freeman, H. J. F. Jansen, and C. L. Fu, Phys. Rev. B **42**, 5433 (1990).

[43] P. F. Carcia, J. Appl. Phys. **63**, 5066 (1988).

[44] R. Wu, C. Li, and A. J. Freeman, J. Magn. Magn. Mater. **99**, 71 (1991).

[45] M. De Santis, A. Buchsbaum, P. Varga, and M. Schmid, Phys. Rev. B **84**, 125430 (2011).

[46] F. Freimuth, Y. Mokrousov, D. Wortmann, S. Heinze, and S. Blügel, Phys. Rev. B **78**, 035120 (2008).

[47] A. A. Mostofi, J. R. Yates, Y.-S. Lee, I. Souza, D. Vanderbilt, and N. Marzari, Comput. Phys. Commun. **178**, 685 (2008).

[48] I. Souza, N. Marzari, and D. Vanderbilt, Phys. Rev. B **65**, 035109 (2001).

[49] C.-F. Pai, L. Liu, Y. Li, H. W. Tseng, D. C. Ralph, and R. A. Buhrman, Appl. Phys. Lett. **101**, 122404 (2012).

[50] For room-temperature measurements on nonannealed AlO_x/Co/Pt trilayers, Ref. [13] reports linear-response coefficients for the effective field per current density j_x of $T_0^{\parallel}/(j_x\mu_S) = 5 \times 10^{-7}$ mT cm^2/A for the longitudinal effective field and $T_0^{\perp}/(j_x\mu_S) = -3.2 \times 10^{-7}$ mT cm^2/A for the transverse effective field. The electrical resistivity of the samples is $\rho_{xx} = 36\ \mu\Omega$ cm. The measured effective fields are the SOTs per magnetic moment. The torkances per magnetic moment are thus $t_{yx}^{\text{even}}/\mu_S = T_0^{\parallel}/(\rho_{xx}\, j_x\, \mu_S) = 0.0139$ mT cm/V and $t_{xx}^{\text{odd}}/\mu_S = T_0^{\perp}/(\rho_{xx}\, j_x \mu_S) = -0.0089$ mT cm/V.

[51] O. Wessely, B. Skubic, and L. Nordström, Phys. Rev. Lett. **96**, 256601 (2006).

[52] P. M. Haney and M. D. Stiles, Phys. Rev. Lett. **105**, 126602 (2010).

[53] G. Y. Guo, S. Murakami, T. W. Chen, and N. Nagaosa, Phys. Rev. Lett. **100**, 096401 (2008).

[54] X. Wang, R. Wu, D.-s. Wang, and A. J. Freeman, Phys. Rev. B **54**, 61 (1996).

[55] J. C. Slonczewski, Phys. Rev. B **39**, 6995 (1989).

[56] P. M. Haney, C. Heiliger, and M. D. Stiles, Phys. Rev. B **79**, 054405 (2009).

[57] G. D. Mahan, *Many-Particle Physics*, Physics of Solids and Liquids (Kluwer Academic/Plenum, New York, 2000).

[58] A. Crépieux and P. Bruno, Phys. Rev. B **64**, 014416 (2001).

[59] A. Bastin, C. Lewiner, O. Betbeder-Matibet, and P. Nozières, J. Phys. Chem. Solids **32**, 1811 (1971).

[60] F. Freimuth, R. Bamler, Y. Mokrousov, and A. Rosch, Phys. Rev. B **88**, 214409 (2013).

[61] F. Freimuth, S. Blügel, and Y. Mokrousov, J. Phys.: Condens. Matter **26**, 104202 (2014).

[62] K. M. D. Hals and A. Brataas, Phys. Rev. B **88**, 085423 (2013).

[63] E. van der Bijl and R. A. Duine, Phys. Rev. B **86**, 094406 (2012).